NeuroImage 249 (2022) 118902

Contents lists available at ScienceDirect

NeuroImage

journal homepage: www.elsevier.com/locate/neuroimage

Evidence for distinct neuro-metabolic phenotypes in humans

Bofan Wu[a], Andrew P. Bagshaw[a], Clayton Hickey[a], Simone Kühn[b,c], Martin Wilson[a,*]

[a] Centre for Human Brain Health and School of Psychology, University of Birmingham, Birmingham, UK
[b] Department of Psychiatry and Psychotherapy, Neuronal Plasticity Working Group, University Medical Center Hamburg-Eppendorf, Germany
[c] Max Planck Institute for Human Development, Lise Meitner Group for Environmental Neuroscience, Germany

ARTICLE INFO

Keywords:
Individual differences
Neurochemical
MR spectroscopy
MRS
ABfit
Spant

ABSTRACT

Advances in magnetic resonance imaging have shown how individual differences in the structure and function of the human brain relate to health and cognition. The relationship between individual differences and the levels of neuro-metabolites, however, remains largely unexplored – despite the potential for the discovery of novel behavioural and disease phenotypes. In this study, we measured 14 metabolite levels, normalised as ratios to total-creatine, with ^{1}H magnetic resonance spectroscopy (MRS) acquired from the bilateral anterior cingulate cortices of six healthy participants, repeatedly over a period of four months. ANOVA tests revealed statistically significant differences of 3 metabolites and 3 commonly used combinations (total-choline, glutamate + glutamine and total-N-acetylaspartate) between the participants, with scyllo-inositol (F=85, p=6e-26) and total-choline (F=39, p=1e-17) having the greatest discriminatory power. This was not attributable to structural differences. When predicting individuals from the repeated MRS measurements, a leave-one-out classification accuracy of 88% was achieved using a support vector machine based on scyllo-inositol and total-choline levels. Accuracy increased to 98% with the addition of total-N-acetylaspartate and myo-inositol – demonstrating the efficacy of combining MRS with machine learning and metabolomic methodology. These results provide evidence for the existence of neuro-metabolic phenotypes, which may be non-invasively measured using widely available 3 Tesla MRS. Establishing these phenotypes in a larger cohort and investigating their connection to brain health and function presents an important area for future study.

1. Introduction

The characterisation of individual differences in brain structure and function is an important goal for neuroscience in order to better understand cognitive and behavioural variations and vulnerabilities to poor physical and mental health. Magnetic resonance techniques are particularly well-suited to the study of individual differences, providing a wealth of structural (Kanai and Rees, 2011) and functional (Finn et al., 2015) information from a single scanning session. For example, individual differences in cortical grey and white matter have been associated with a range of behavioural measures, including decision making (van Gaal et al., 2011, p.), general intelligence (Haier et al., 2004), personality traits (DeYoung et al., 2010), reaction time (Tuch et al., 2005) and bimanual co-ordination (Johansen-Berg et al., 2007) tasks. Similarly, differences in functional connectivity can explain variance in lifestyle, demographic and psychometric factors (Smith et al., 2015). Structural and functional information is not redundant, suggesting that quantification of different physiological variables will help to explain an increasingly high proportion of the behavioural variance between individuals.

MR is an extremely versatile technique, and in addition to structural and functional information from MR imaging, MR spectroscopy (MRS) provides a complementary view of the brain. The most common technique, ^{1}H MRS, can measure a range of key metabolites within the human brain, offering unique insight into the metabolic state of neural tissue. The localised level of one of the most readily observed metabolites, N-acetylaspartate, has been associated with several measures of cognition, including fluid intelligence (Nikolaidis et al., 2017), cognitive performance (Jung et al., 1999) and creativity (Jung et al., 2009) – highlighting the efficacy of MRS in characterising individual differences in higher order cognitive processing. It is also possible to measure the primary inhibitory neurotransmitter in the mature human brain, Gamma-Aminobutyric acid (GABA), with edited MRS acquisition techniques (Mescher et al., 1998), and the resting-state level of GABA has been correlated with individual differences in motor reaction times (Stagg et al., 2011), visual orientation discrimination (Edden et al., 2009), tactile discrimination (Puts et al., 2011) and motor decision speed (Sumner et al., 2010).

Despite these studies, individual differences in neurometabolic profiles, as measured with MRS, remain underexplored relative to anatomi-

* Corresponding author.
E-mail address: wilsonmp@bham.ac.uk (M. Wilson).

https://doi.org/10.1016/j.neuroimage.2022.118902.
Received 28 May 2021; Received in revised form 5 January 2022; Accepted 9 January 2022
Available online 13 January 2022.

Table 1
A summary of the MRS data acquired for each of the 6 study participants. GM fraction is the ratio of grey matter to white matter contained within the MRS acquisition region. Water supp. eff. is the efficiency of the water suppression measured from the relative heights of the water signals in the water supressed and water reference data.

		GM fraction (%)		spectral SNR		linewidth (ppm)		water supp. eff. (%)	
participant	N	mean	s.d.	mean	s.d.	mean	s.d.	mean	s.d.
1	8	72	3.1	172	14	0.037	0.0028	0.46	0.07
2	13	70	5.3	142	17	0.043	0.0043	0.95	0.56
3	11	70	2.3	153	21	0.041	0.0074	0.45	0.09
4	12	75	4.4	147	14	0.036	0.0044	0.64	0.15
5	11	70	6.2	133	22	0.044	0.0078	0.47	0.11
6	11	72	1.5	167	14	0.037	0.0041	0.51	0.07

cal, diffusion and functional MRI. Previous investigation has focussed on individual metabolite levels, bypassing one of the primary strengths of MRS: the ability to measure multiple metabolites simultaneously. Multivariate analysis of metabolite "profiles" for phenotype discovery is well-established in the field of metabolomics, where biofluids such as urine and blood plasma are known to have metabolic features specific to an individual that remain stable over a period of months (Assfalg et al., 2008). Whilst urine and blood samples are convenient to collect and analyse, their relevance to neuro-metabolism is unknown and likely confounded by the blood-brain barrier. In contrast, MRS provides direct measurement of endogenous cytosolic brain metabolites and would therefore be expected to have greater sensitivity and relevance in detecting and interpreting individual differences in neuro-metabolism.

In this work, we seek to demonstrate the existence of neurometabolic phenotypes which distinguish individuals with high precision and remain stable over a period of months. MRS was acquired from the bilateral anterior cingulate cortices of six healthy participants over a period of four months, measured as part of the day2day study (Filevich et al., 2017). Using advanced spectral analysis and conventional machine learning techniques, we show how combining multiple metabolite levels yields high classification accuracy between participants – providing novel evidence for the existence of neuro-metabolic phenotypes.

2. Methods

2.1. Participants and MR acquisition protocol

Eight participants (six female) took part in the day2day study (Filevich et al., 2017) and were scanned with an imaging protocol including MRS over a period of four months. Insufficient MRS data (N < 3) was acquired for two participants and these were excluded from further analysis, leaving six participants (five female) who were scanned an average of 11 times over the study period.

MRI and MRS were collected on a 3T Magnetom Trio MRI scanner system (Siemens Medical Systems, Erlangen, Germany) using a 12-channel radiofrequency head coil. The fMRI stability quality assurance procedure (Friedman and Glover, 2006) was performed weekly, to ensure consistency of the MR measurements, and no major hardware or software changes were made over the study period.

A T1 weighted anatomical MRI scan (MPRAGE) was acquired at each session with the following sequence parameters: TR = 2500 ms, TE = 4.77 ms, TI = 1100 ms, FOV = 256 × 256 × 192 mm^3, flip angle = 7°, bandwidth = 140 Hz/pixel, 1 × 1 × 1 mm^3 voxel size, 9:20 min duration. A single voxel MRS PRESS acquisition volume (25 × 30 × 20 mm^3) was placed on the bilateral ACC (Figure 1A) and both water suppressed (128 averages) and water reference (8 averages) were acquired from the same region. The following MRS sequence parameters were used: TR = 3000 ms, TE = 80 ms, flip angle = 90°, 2048 complex data points, 2500Hz spectral width, "advanced" automated shimming, 6:36 min duration. Water suppression was performed with the vendor implementation of CHESS (Haase et al., 1985). An intermediate echo-time of 80 ms was chosen based on its particular efficacy for the detection of glutamate at 3 Tesla (Schubert et al., 2004) and the general reduction of spectral interference from macromolecules and residual water associated with longer echo-times.

Further details on participants and the MR acquisition protocol is available in the day2day investigation paper (Filevich et al., 2017). The day2day study was approved by The Ethics Committee of Charité University Clinic, Berlin.

2.2. MR spectroscopy analysis

Raw MRS data were processed and analysed with the spant analysis package (Wilson, 2021a). Following coil combination, individual transients were aligned using the RATS method (Wilson, 2019) and automated spectral fitting was performed with the ABfit algorithm (Wilson, 2021b). A simulated basis set was used for analysis containing the following set of standard metabolites: alanine (Ala), aspartate (Asp), creatine (Cr), gamma-Aminobutyric acid (GABA), glucose (Glc), glutamine (Gln), glutathione (GSH), glutamine (Gln), glycerophosphocholine (GPC), myo-inositol (Ins), lactate (Lac), N-acetylaspartate (NAA), N-acetylaspartylglutamate (NAAG), phosphocholine (PCho), phosphocreatine (PCr), scyllo-inositol (sIns) and taurine (Tau). The following standard combinations of metabolites were used in subsequent analysis due to high spectral interference: N-acetylaspartate + N-acetylaspartylglutamate (tNAA); phosphocholine + glycerophosphocholine (tCho); creatine + phosphocreatine (tCr) and glutamate + glutamine (Glx). The commonly used set of broad signals to model macromolecular and lipid signals present in ^{1}H MRS data were also included in the basis set, see Table 1 of (Wilson et al., 2011) for the full listing. Baseline modelling was performed using the adaptive penalised spline method (Wilson, 2021b), without modification to any of the default constraint parameters. Metabolite levels were normalised as ratios to tCr to eliminate the influence of CSF on metabolite level estimates. Additional analysis was performed on metabolite levels scaled to the water reference signal, as described in (Gasparovic et al., 2006), to evaluate the influence of using tCr as a common scaling factor.

The spectral signal-to-noise ratio (SNR) was measured from the peak height of the tNAA resonance and the noise region between -0.5 and -2.5 ppm. Spectral linewidth was estimated from the full width half maximum of the tNAA resonance and the water suppression efficiency was measured as a ratio between the magnitude peak heights of the water resonance in the suppressed and unsuppressed spectra (Kreis et al., 2020). All spectra were visually assessed for artefacts.

Cramér–Rao lower bounds (CRLBs) were calculated to estimate the accuracy of each metabolite level. CRLB standard deviation estimates were converted to a percentage error and the mean calculated for each participant. The lowest mean percentage CRLB for each metabolite across participants was taken as a measure of accuracy. Accuracy was calculated in this way to prevent participants with systemically a low metabolite level, and therefore high percentage error, from dominating the estimate. Metabolite estimates with an amplitude of zero had a

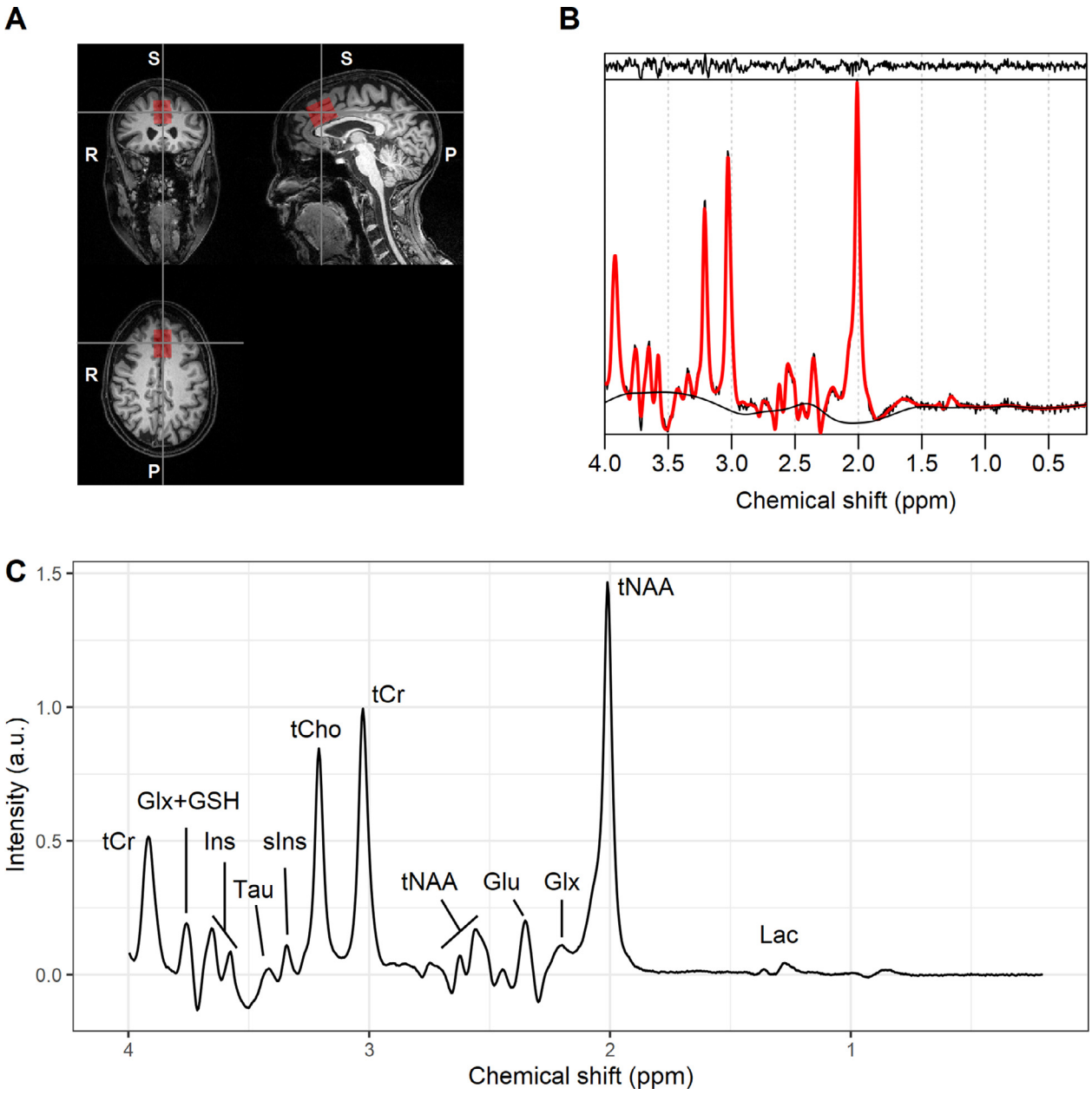

Fig. 1. A) MRS voxel positioning in the bilateral ACC region shown on a T1 weighted MPRAGE scan from participant 2. B) ABfit analysis result, from the same scanning session as part A), with the baseline and fit residual shown in black as the bottom and top traces respectively. C) Mean spectrum (N=66) calculated following baseline subtraction and normalisation to the height of the tCr resonance.

percentage error of infinity and were not included in the above calculation. Any metabolites with a mean percentage CRLB greater than 50% were excluded from further analysis. Furthermore, the following individual metabolites, which are known to strongly overlap, were excluded and replaced with the standard set of combinations listed above: NAA, NAAG, Cr, PCr, GPC, PCho, Glu, Gln.

The MRS acquisition voxel was spatially mapped to the volumetric T1 data with the spant software package, and percentages of white matter, grey matter and CSF calculated from tissue segmentation performed with the FAST (Zhang et al., 2001) method – implemented as part of the FSL package (Woolrich et al., 2009). . Each voxel position was manually assessed for accuracy, and positioning errors causing a displacement of greater than 5 mm in any direction were excluded from further analysis.

2.3. Neuro-metabolic phenotyping

To establish a neuro-metabolic phenotype we sought metabolite levels that: 1) have high discriminatory value in distinguishing between individuals and 2) are stable over a period of months. The stability and inter-participant variability of each individual metabolite level was evaluated with one-way ANOVA, using participant level groupings, as an initial exploratory step. For example, the strength and likelihood of a genuine difference in the mean value of tNAA between each participant is related to the ANOVA F-statistic and p-value respectively.

In addition to measured metabolite levels, one-way ANOVA was also performed directly on each spectral data point (following automated spectral alignment and phasing with RATS and ABfit) over the default fitting range between 0.2 and 4 ppm to corroborate the metabolite level

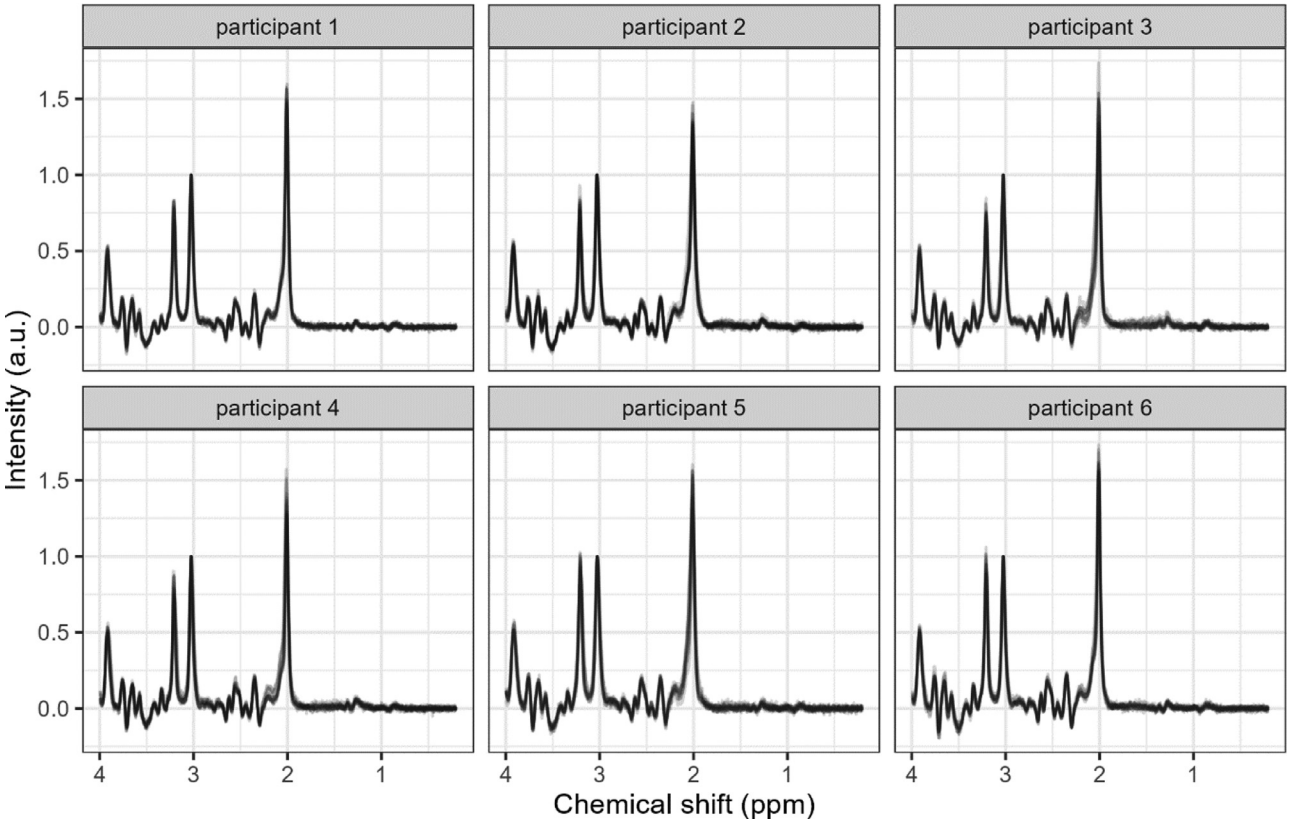

Fig. 2. All spectra with acceptable quality (N = 66), overlayed and split across the participants to visually evaluate spectral stability. Each spectrum is plotted with partial transparency to illustrate the consistency between sessions. Frequency and phase correction were performed automatically and baseline estimates were subtracted to reduce variance from residual water. Spectra are normalised to the height of the tCr resonance at 3.03 ppm.

analysis. The resultant F-values may be plotted to establish the most important spectral regions for distinguishing between each participant, providing a complementary metabolic analysis independent from the assumptions and potential bias of spectral fitting algorithms.

Supervised machine leaning was used to determine if multiple metabolite levels could be combined to classify individuals, thereby establishing the existence of a temporally stable neuro-metabolic phenotype for the six individuals studied. A support-vector machine learning algorithm with a linear kernel was applied to various combinations of metabolite levels and classification accuracy was assessed using leave-one-out cross-validation. Training, classification and validation step were performed using the mlr3 (Lang et al., 2019) R package and the LIBSVM library (Chang and Lin, 2011).

An unsupervised principal component analysis was also performed to explore the proportion of variance in metabolite levels that may be attributed to individual differences. The full set of metabolites, as listed above, were included in the analysis as ratios to total-creatine, however strongly overlapping resonances, such as glutamate and glutamine, were replaced with their combined levels (e.g. Glx). Metabolite levels were each centred to have a mean of zero and scaled to unit variance prior to principal components analysis.

All MRS analysis, statistics and machine-learning was performed with the R statistical computing platform (R Core Team, 2021) and analysis scripts used to generate the figures and tables in this paper will be available from https://github.com/martin3141/neuro_metabolic_phenotyping upon publication. The day2day dataset, including the MRS and MRI data presented here, is freely available for usage in scientific research. To prevent its circulation unrelated to research usage, we ask that scientists interested in obtaining the dataset email author (SK) directly.

3. Results

A total of 69 spectra were available for analysis. All fitting results and voxel locations were manually inspected to confirm the absence of significant spectral artefacts and appropriate positioning of the MRS acquisition region on the T1 anatomical scan. An example is shown in Fig. 1. Three spectra were discarded for having: 1) poor linewidth (0.07 ppm) relative to the other data; 2) incorrect voxel positioning and 3) a strong artefact from a spurious residual water echo. Supplementary Fig. 2 shows each voxel position for subject 3 and the excluded scan due to incorrect placement. The remaining 66 spectra were distributed among the 6 participants as listed in Table 1. The date of each scan is shown in Supplementary Fig. 2 and the mean duration between the first and last scan for each participant was 78 days. Spectral quality was very high with a mean linewidth of 0.04 ppm and mean SNR of 151 over all 66 spectra. CRLB based error estimates for each metabolite, as described in the previous section, are listed in Supplementary Table 1, with Tau, GABA, Glc, Lac and Ala being removed from further analysis due to their estimated errors being greater than 50%.

Phase, frequency and baseline corrected spectra, as determined as part of the automated processing pipeline (Wilson, 2021b, 2019), are shown in Fig. 2. Each spectrum is plotted with transparency and grouped by participant to illustrate the high consistency in data quality, and to highlight the presence of any strong spectral features with the potential to discriminate between the participants. For example, the ratio between the tCho / tCr resonances, at 3.2 and 3.03 ppm respectively, appears characteristically elevated in participants 5 and 6 relative to participants 1 and 3.

Whilst informative, the visual assessment of individual differences in spectral appearance is inherently biased towards higher concentra-

Table 2
ANOVA summary statistics for each metabolite quantity to evaluate the difference in mean metabolite levels between the 6 participants studied. Values in bold are below the Bonferroni corrected p-value of 0.0071.

metab. / tCr	F-statistic	p-value
sIns	85.0	**6.34e-26**
tCho	39.2	**1.13e-17**
Ins	20.9	**5.07e-12**
Glx	19.9	**1.24e-11**
tNAA	8.2	**5.66e-06**
Asp	4.9	**8.18e-04**
GSH	1.9	1.02e-01

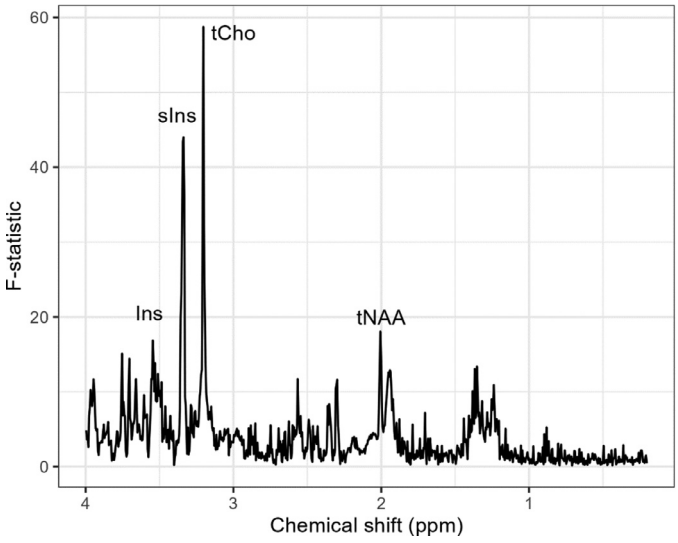

Fig. 3. Spectral ANOVA results performed on each frequency domain point independently and grouped over participants (as shown in Fig. 2). Large F-statistic values correspond to a strong differences in the mean spectral intensity between participants. Predominant spectral differences between participants are clear at 3.35 and 3.2 ppm, assigned as sIns and tCho respectively, in good agreement with the metabolite fitting results listed in Table 2.

tion metabolites with multiple equivalent protons, such as the primary singlet resonances from tNAA, tCr and tCho. One-way ANOVA was applied in a univariate fashion (once for each metabolite) to explore the discriminatory value of each metabolite, where a larger F-statistic indicates a more likely difference in mean metabolite levels between participants. Table 2 shows strong differences in the levels of multiple metabolites indicating a large proportion of the variance in the observed metabolite levels can be attributed to individual differences in neurometabolism – which were stable over the MRS data acquisition period of four months. Supplementary Table 2 shows the same analysis but performed on concentration estimates derived from water reference based scaling (Gasparovic et al., 2006) – rather than metabolite levels as ratios to tCr. Good agreement was found between both analyses, and while tCr was found to differ between individuals (F=9.4) very strong effects remained for both sIns (F=71.1) and tCho (F=63.7).

The sIns and tCho metabolites had the strongest discriminatory value, with both primary resonances being observable at 3.35 and 3.2 ppm respectively (Fig. 2). A further confirmatory analysis was performed by performing one-way ANOVA directly on the processed spectral data to highlight frequency ranges related to individual differences, and significantly reduce any potential confounds related to biases or instabilities in the fitting procedure. Strong agreement was found between the spectral (Fig. 3) and fitted metabolite (Fig. 2) ANOVA results – with both analyses finding sIns and tCho as the most discriminatory spectral regions and metabolite levels. Coefficients of variation for each metabolite are listed in Supplementary Table 3, with sIns and tCho having mean coefficients of 12.6 % and 5.7 % respectively when averaged across the six participants.

The ability of one or more neuro-metabolites to uniquely distinguish or characterise individuals may be framed as a classification problem, and therefore suited to a machine learning approach. A simple classification model, based on the two most effective univariate predictor variables: tCho and sIns (Table 2), was used to confirm the efficacy of combining one or more MRS derived neuro-metabolites to predict the donor participant. A support vector machine learning model, with a linear kernel, was applied to the tCho and sIns predictors (as ratios to tCr) and a high classification accuracy of 88% was achieved – as measured with leave-on-out cross-validation. Fig. 4 shows the classification decision boundaries and predicted classes of the 68 donor spectra. Most data points cluster about distinct centroids attributable to each participant.

A second exploratory classification model was implemented with the same methodology but including additional metabolites to investigate how the use of a more complete metabolite "profile" may be used to improve classification accuracy. The combination of tCho, sIns, tNAA and Ins (as ratios to tCr) yielded an improved leave-one-out accuracy of 98% – relative to the previous two-feature model.

The results of an unsupervised principal component analysis performed on the statistically significant metabolite levels (see Table 2) are shown in Fig. 5. Part A) shows reasonable separation between participants 2, 3 and 6 may be achieved by comparing PC1 vs PC2, which together account for 63% of the total variance in the dataset, whereas PC1 vs PC3 (part B) shows improved separation for participant 1. The loadings arrows in parts A) and B) indicate that scyllo-inositol and total-choline each contribute primarily to PC1 and PC3, implying temporally stable individual differences are one of the primary sources of variance in neuro-metabolite levels.

Small differences in the mean levels of grey matter tissue included in the MRS acquisition region are seen in Table 1 – with a range of 6%. These differences are likely due to minor variations in the subject's bilateral ACC anatomy, for example cortical thickness and sulcal patterns. Since metabolite levels are known to vary between grey and white matter (Wang and Li, 1998), we explored the association between the levels of grey matter voxel composition and metabolite values. Fig. 6 shows no significant link between the grey matter fraction and sIns and tCho, indicating that genuine changes in neuro-metabolism are the cause of the observed individual differences in metabolite levels, rather than variations in neuroanatomy.

4. Discussion

Our results show it is possible to accurately characterise an individual based on their neuro-metabolic profile, as measured non-invasively with MRS. The stability of this profile, over a period of months, provides new evidence for the existence of a neurometabolic phenotype in humans, with scyllo-inositol, total-choline and total-creatine acting as the dominant metabolic features in the bilateral ACC brain region. We also show how the addition of tNAA and myo-inositol levels confers a more precise characterisation and, more generally, how combining MRS derived neurometabolic profiles with machine learning is an important and currently underused tool in neuroscience and neuropathology.

Our observation that scyllo-inositol is characteristically different between individuals and stable over a period of months is novel and not readily explained by other studies. The age range of our cohort was too narrow (24-32 years) for differences to be congruent with changes previously linked to normal aging (Kaiser et al., 2005), and the volunteers' alcohol consumption was significantly below the levels associated with alcoholic metabolic encephalopathy (Viola et al., 2004). Large elevations in the scyllo-inositol to myo-inositol ratio have been reported for a single healthy individual when compared to normative levels, as observed in this study and others, suggesting these two molecules are regulated independently and large relative deviations are compatible

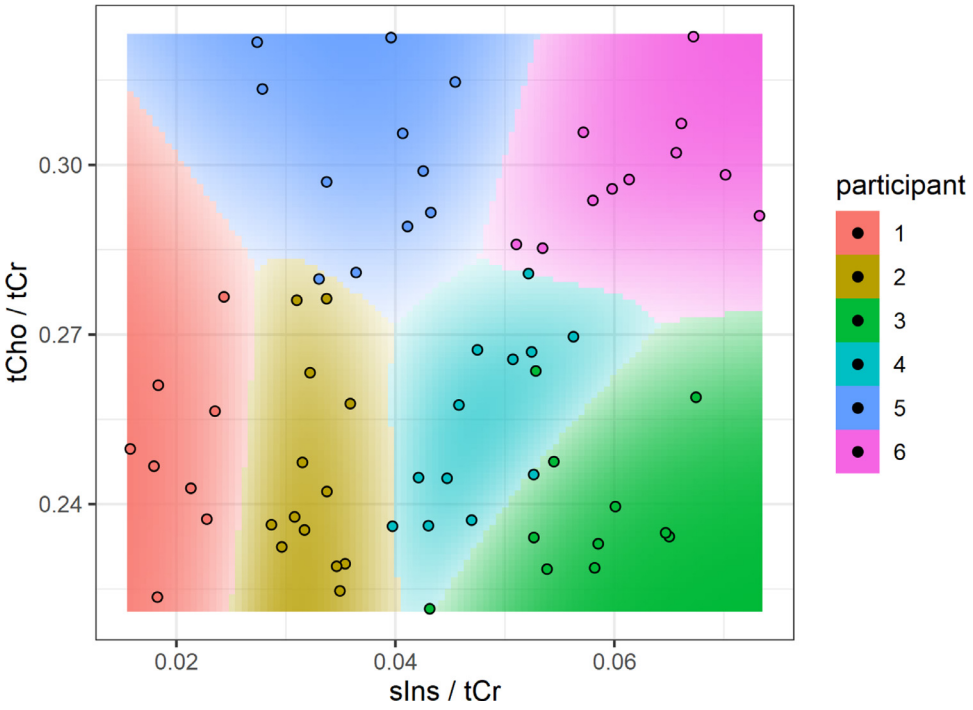

Fig. 4. Decision boundary plot for the support vector machine classifier model applied to tCho/tCr and sIns/tCr. Leave-one-out accuracy was 88%.

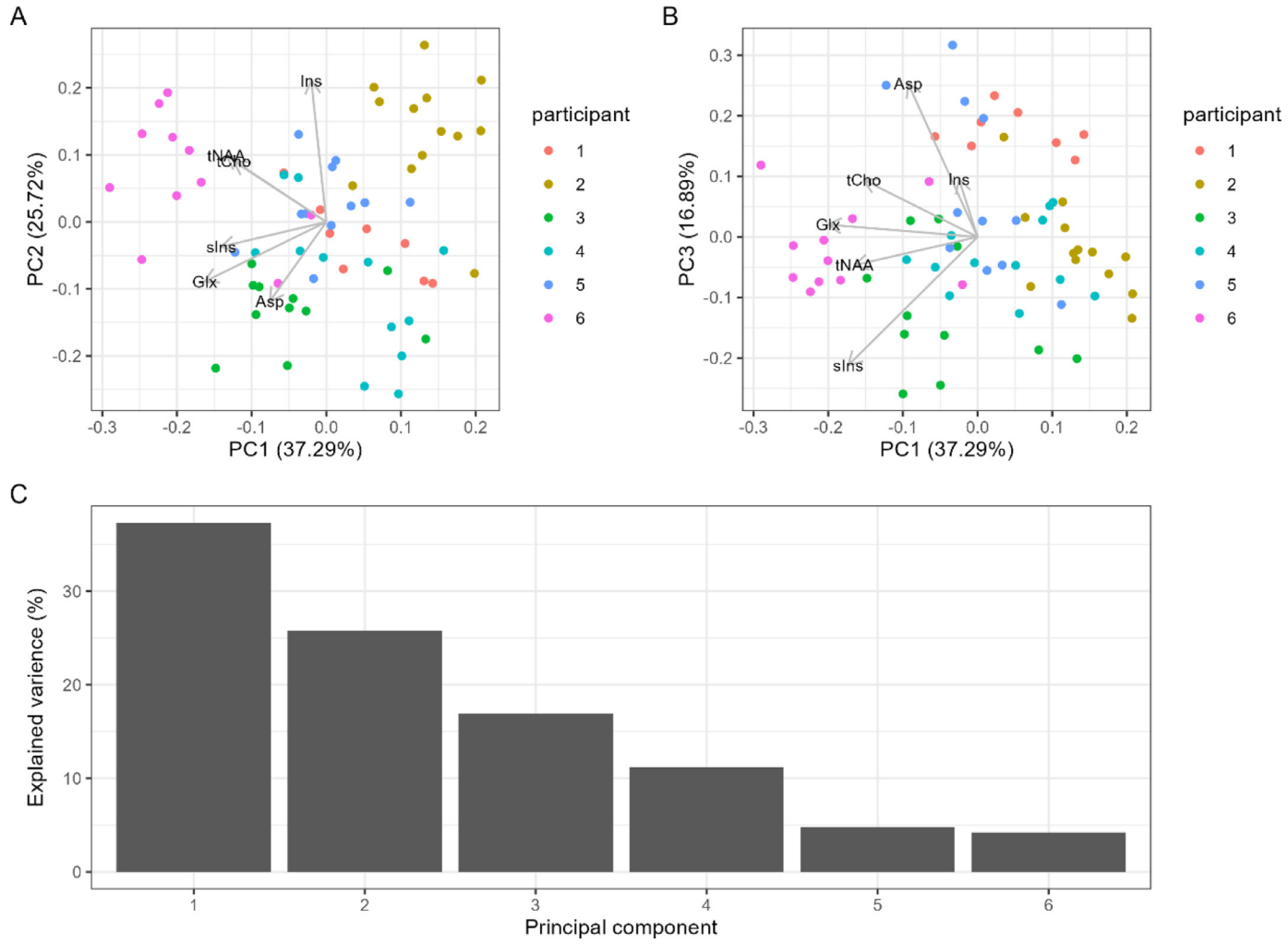

Fig. 5. Principal component analysis of metabolite levels as ratios to total-creatine. PC1 vs PC2 and PC1 vs PC3 scores plotted as points in parts A) and B) respectively, with metabolite loadings represented as grey arrows. Percentages of the explained variance for each principal component are shown in part C).

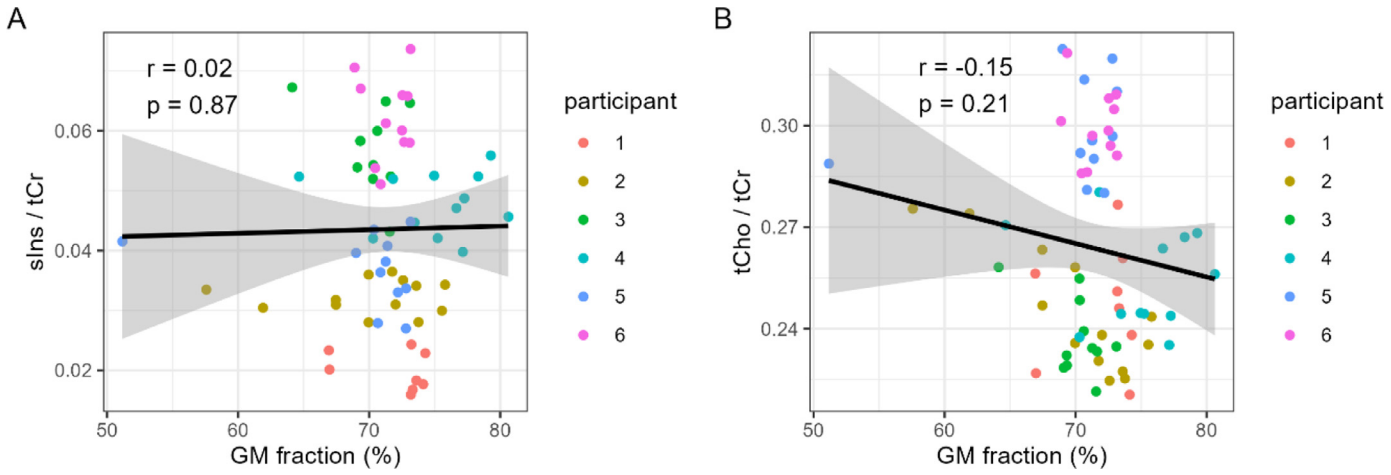

Fig. 6. Scatter plot of the relationship between the primary distinguishing metabolite features and the proportion of grey matter in the MRS acquisition region. The absence of any correlation suggests gross anatomical features are not the primary source of variance in these metabolite quantities.

with healthy brain function (Seaquist and Gruetter, 1998). This large elevation in scyllo-inositol was also found to be stable over a period of 12 months, in agreement with our results. The relatively high concentration of scyllo-inositol in some fruit juices suggests diet may be one potential source of variability (Sanz et al., 2004). This, combined with an association between fruit juice consumption and improved cognitive function in healthy middle-aged males (Alharbi et al., 2016) promotes scyllo-inositol as an interesting new biomarker for further study – potentially providing a mechanistic link between diet and healthy cognitive ageing (Lamport et al., 2014).

In addition to scyllo-inositol, several other metabolites were found to differ between participants – including tNAA, tCho and myo-inositol. Numerous studies have shown how these commonly measured metabolites alter with pathology (Oz et al., 2014), however their precise role in healthy brain tissue remains unclear. These metabolites levels are known to differ between neuro-cellular types (Urenjak et al., 1993) and their levels may therefore relate to individual differences in grey matter tissue composition. For example, tNAA and myo-inositol are generally considered to be approximate markers of neuronal and glial cell types and their concentrations may reflect the relative proportions or metabolic state of these cells within the bilateral ACC MRS acquisition volume.

A PRESS sequence with an intermediate echo-time of 80 ms was used for this study. This echo-time is known to be advantageous due to the suppression of interfering macromolecular signals, thereby reducing the need for an echo-time specific macromolecular signal model. However, intermediate echo-times are also associated with reduced metabolite signal intensity arising from increased T2 relaxation and a general dephasing of J-coupled metabolite resonances, e.g., myo-inositol, phosphoethanolamine and ascorbate. Furthermore, the localisation quality of commercial PRESS implementations are known to be poor at 3 Tesla and above (Wilson et al., 2019). More modern acquisition methods, such as semi-LASER or SPECIAL (Öz et al., 2021), combined with a short TE protocol and improved macromolecular modelling (Cudalbu et al., 2021) should be preferred for future studies for improvements in both signal localisation and metabolite detection accuracy.

MRS derived metabolite measures are commonly expressed either as ratios, e.g., tNAA/tCr, or as concentrations based on information available from a water reference scan (Near et al., 2021). Both approaches have strengths and limitations, with the ratio method being simple to implement, but making interpretation difficult in the case when both contributing measures are known to vary. Conversely, the water reference approach simplifies interpretation, but potentially erroneous assumptions about the water content of tissue and relative relaxation rates are required. In the case of MRSI, metabolite ratios are more commonly used since water reference data are more time consuming to acquire and therefore less likely to be available. In this study, primary analysis was performed on metabolite ratios to tCr, however a secondary analysis showed the findings to be consistent with water referenced metabolite levels (see Table 2 vs Supplementary Table 2). Agreement between the two different approaches provides evidence our findings are robust, and that either method is suitable for neuro-metabolic profiling.

Systematic differences in data quality between participants have the potential to introduce biases in metabolite levels during fitting, resulting in erroneous discriminatory metabolite markers. Supplementary Table 4 shows systematic differences in SNR, water suppression efficiency and tNAA linewidth were present in our data, however the effect sizes (F=7.3, 6.5, 4.5) were small relative to the top three discriminatory metabolite markers (F > 20) and we therefore conclude data quality is highly unlikely to be driving these differences in metabolite levels. Furthermore, Fig. 2 shows stable baselines across the full spectral range, indicating baseline distortions from residual water signal were not high enough to influence metabolite fitting. Fig. 3 shows how a simpler spectral analysis agrees with the results from metabolite fitting, giving further evidence that fitting biases caused by differences in data quality are unlikely to be driving the observed metabolite differences. Underlying factors that may explain the systematic differences in SNR, tNAA linewidth and residual water include: 1) relative differences in the tNAA signal strength, 2) the ratio between NAA and NAAG and 3) the proportion of CSF in the MRS voxel.

Whilst this work presents new evidence for the existence of neurometabolic phenotypes, one of its primary limitations is the low number of participants studied (N = 6). Attempts to discount trivial and systematic factors driving metabolite differences (e.g. differences in brain morphology or participant head motion) will be heavily underpowered, therefore our results provide a strong justification for studies with a greater number of participants. A further limitation is the investigation of a single brain region. Regional variations in metabolite levels have been established with MR spectroscopic imaging (MRSI), showing differences of up 10% in tNAA between the left and right cerebral hemispheres and a trend towards increasing levels from the anterior to posterior cerebrum (Maudsley et al., 2009). Whilst MRSI is prone to reduced data quality, compared to single voxel MRS (Wilson et al., 2019), this loss may be mitigated by the addition of spatial information – ultimately improving individual characterisation.

The cognitive implications of these individual differences in metabolite profiles presents an important area for future study. The levels of frontal-parietal tNAA have been shown to predict fluid intelligence

(Nikolaidis et al., 2017), and follow different age related changes between adults with autism spectrum disorders compared to those with typical development (Aoki et al., 2012). The relationship between emotional traits and MRS acquired from the right dorsal anterior cingulate cortex has also been recently reported (White et al., 2021), where tNAA was found to correlate with Absorption and Aggression, as measured by the Multidimensional Personality Questionnaire Brief Form (Patrick et al., 2002). Glx and tCho were also associated with behavioural flexibility and social affiliation, however these relationships had a smaller effect size and were not statistically significant following correction for multiple comparisons. These results, combined with our findings, justify much larger studies to explore how the neurometabolic profiles from multiple brain regions, as measured with MRSI, relate to contextual changes in cognition and personality and to stability in such traits over time.

The two metabolites with the most discriminatory power between participants were scyllo-inositol and tCho, and notably both these metabolites have been associated with ageing and cognitive decline. Dietary choline has been associated with improved performance in cognitive tasks for middle-aged and older men, with greater choline intake found to correlate with verbal fluency and memory function (Ylilauri et al., 2019). Dietary choline supplementation has also been shown to improve spatial memory and beta-amyloid load in an Alzheimer's Disease mouse model (Velazquez et al., 2019). Increases in scyllo-inositol are associated with ageing (Kaiser et al., 2005) and dietary supplantation has been shown to ameliorate impaired cognition in a Alzheimer's Disease mouse model (McLaurin et al., 2006). The ability of MRS to detect these neuro-metabolic markers in-vivo presents a compelling potential diagnostic technique to detect the early stages of cognitive decline, and future work should be undertaken to explore the connection between these markers, diet and cognitive changes associated with ageing.

In conclusion, we have shown how combining MRS with machine learning may be used to derive temporally stable neuro-metabolic profiles from healthy adults. The high classification accuracy achieved in discriminating between six participants provides novel evidence for the existence of neuro-metabolic phenotypes, and future work is warranted to investigate a greater number of individuals and explore how these findings relate to the wider adult population, cognitive function and brain health.

Credit authorship contribution statement

Bofan Wu: Formal analysis, Investigation. Andrew Bagshaw: Conceptualization, Writing - Review & Editing. Clayton Hickey: Conceptualization, Writing - Review & Editing. Simone Kühn: Resources, Data Curation, Writing - Review & Editing. Martin Wilson: Conceptualization, Supervision, Software, Writing - Original Draft, Formal analysis, Investigation, Methodology.

Analysis scripts used to generate the Fig.s and tables in this paper will be available from https://github.com/martin3141/neuro_metabolic_phenotyping upon publication. The day2day dataset is freely available for usage in scientific research. To prevent its circulation unrelated to research usage, we ask that scientists interested in obtaining the dataset email author (SK) directly.

Declaration of Competing Interest

The authors declare no conflict of interest.

Acknowledgements

This work was supported by a H2020 European Research Council Starting Grant [grant number 804360-INSENSE].

Supplementary materials

Supplementary material associated with this article can be found, in the online version, at doi:10.1016/j.neuroimage.2022.118902.

References

Alharbi, M.H., Lamport, D.J., Dodd, G.F., Saunders, C., Harkness, L., Butler, L.T., Spencer, J.P.E., 2016. Flavonoid-rich orange juice is associated with acute improvements in cognitive function in healthy middle-aged males. Eur. J. Nutr. 55, 2021–2029. doi:10.1007/s00394-015-1016-9.

Aoki, Y., Abe, O., Yahata, N., Kuwabara, H., Natsubori, T., Iwashiro, N., Takano, Y., Inoue, H., Kawakubo, Y., Gonoi, W., Sasaki, H., Murakami, M., Katsura, M., Nippashi, Y., Takao, H., Kunimatsu, A., Matsuzaki, H., Tsuchiya, K.J., Kato, N., Kasai, K., Yamasue, H., 2012. Absence of age-related prefrontal NAA change in adults with autism spectrum disorders. Transl Psychiatry 2, e178. doi:10.1038/tp.2012.108.

Assfalg, M., Bertini, I., Colangiuli, D., Luchinat, C., Schäfer, H., Schütz, B., Spraul, M., 2008. Evidence of different metabolic phenotypes in humans. Proc. Natl. Acad. Sci. U. S. A. 105, 1420–1424. doi:10.1073/pnas.0705685105.

Chang, C.-C., Lin, C.-J., 2011. LIBSVM: A library for support vector machines. ACM Trans. Intell. Syst. Technol. 2. doi:10.1145/1961189.1961199, 27:1-27:27.

Cudalbu, C., Behar, K.L., Bhattacharyya, P.K., Bogner, W., Borbath, T., de Graaf, R.A., Gruetter, R., Henning, A., Juchem, C., Kreis, R., Lee, P., Lei, H., Marjańska, M., Mekle, R., Murali-Manohar, S., Považan, M., Rackayová, V., Simicic, D., Slotboom, J., Soher, B.J., Starčuk, Z., Starčuková, J., Tkáč, I., Williams, S., Wilson, M., Wright, A.M., Xin, L., Mlynárik, V., 2021. Contribution of macromolecules to brain 1 H MR spectra: Experts' consensus recommendations. NMR Biomed. 34, e4393. doi:10.1002/nbm.4393.

DeYoung, C.G., Hirsh, J.B., Shane, M.S., Papademetris, X., Rajeevan, N., Gray, J.R., 2010. Testing predictions from personality neuroscience. Brain structure and the big five. Psychol. Sci. 21, 820–828. doi:10.1177/0956797610370159.

Edden, R.A.E., Muthukumaraswamy, S.D., Freeman, T.C.A., Singh, K.D., 2009. Orientation discrimination performance is predicted by GABA concentration and gamma oscillation frequency in human primary visual cortex. J. Neurosci. 29, 15721–15726. doi:10.1523/JNEUROSCI.4426-09.2009.

Filevich, E., Lisofsky, N., Becker, M., Butler, O., Lochstet, M., Martensson, J., Wenger, E., Lindenberger, U., Kühn, S., 2017. Day2day: investigating daily variability of magnetic resonance imaging measures over half a year. BMC Neurosci. 18, 65. doi:10.1186/s12868-017-0383-y.

Finn, E.S., Shen, X., Scheinost, D., Rosenberg, M.D., Huang, J., Chun, M.M., Papademetris, X., Constable, R.T., 2015. Functional connectome fingerprinting: identifying individuals using patterns of brain connectivity. Nat. Neurosci. 18, 1664–1671. doi:10.1038/nn.4135.

Friedman, L., Glover, G.H., 2006. Report on a multicenter fMRI quality assurance protocol. J. Magn. Reson. Imaging 23, 827–839. doi:10.1002/jmri.20583.

Gasparovic, C., Song, T., Devier, D., Bockholt, H.J., Caprihan, A., Mullins, P.G., Posse, S., Jung, R.E., Morrison, L.A., 2006. Use of tissue water as a concentration reference for proton spectroscopic imaging. Magn. Reson. Med. 55, 1219–1226. doi:10.1002/mrm.20901.

Haase, A., Frahm, J., Hänicke, W., Matthaei, D., 1985. 1H NMR chemical shift selective (CHESS) imaging. Phys. Med. Biol. 30, 341–344. doi:10.1088/0031-9155/30/4/008.

Haier, R.J., Jung, R.E., Yeo, R.A., Head, K., Alkire, M.T., 2004. Structural brain variation and general intelligence. Neuroimage 23, 425–433. doi:10.1016/j.neuroimage.2004.04.025.

Johansen-Berg, H., Della-Maggiore, V., Behrens, T.E.J., Smith, S.M., Paus, T., 2007. Integrity of white matter in the corpus callosum correlates with bimanual co-ordination skills. Neuroimage 36 (Suppl 2), T16–T21. doi:10.1016/j.neuroimage.2007.03.041.

Jung, R.E., Gasparovic, C., Chavez, R.S., Flores, R.A., Smith, S.M., Caprihan, A., Yeo, R.A., 2009. Biochemical Support for the "Threshold" Theory of Creativity: A Magnetic Resonance Spectroscopy Study. J. Neurosci. 29, 5319–5325. doi:10.1523/JNEUROSCI.0588-09.2009.

Jung, R.E., Yeo, R.A., Chiulli, S.J., Sibbitt, W.L., Weers, D.C., Hart, B.L., Brooks, W.M., 1999. Biochemical markers of cognition: a proton MR spectroscopy study of normal human brain. Neuroreport 10, 3327–3331. doi:10.1097/00001756-199911080-00014.

Kaiser, L.G., Schuff, N., Cashdollar, N., Weiner, M.W., 2005. Scyllo-inositol in normal aging human brain: 1H magnetic resonance spectroscopy study at 4 Tesla. NMR Biomed. 18, 51–55. doi:10.1002/nbm.927.

Kanai, R., Rees, G., 2011. The structural basis of inter-individual differences in human behaviour and cognition. Nat. Rev. Neurosci. 12, 231–242. doi:10.1038/nrn3000.

Kreis, R., Boer, V., Choi, I.-Y., Cudalbu, C., de Graaf, R.A., Gasparovic, C., Heerschap, A., Krššák, M., Lanz, B., Maudsley, A.A., Meyerspeer, M., Near, J., Öz, G., Posse, S., Slotboom, J., Terpstra, M., Tkáč, I., Wilson, M., Bogner, W.Experts' Working Group on Terminology for MR Spectroscopy, 2020. Terminology and concepts for the characterization of in vivo MR spectroscopy methods and MR spectra: Background and experts' consensus recommendations. NMR Biomed. e4347. doi:10.1002/nbm.4347.

Lamport, D.J., Saunders, C., Butler, L.T., Spencer, J.P., 2014. Fruits, vegetables, 100% juices, and cognitive function. Nutr. Rev. 72, 774–789. doi:10.1111/nure.12149.

Lang, M., Binder, M., Richter, J., Schratz, P., Pfisterer, F., Coors, S., Au, Q., Casalicchio, G., Kotthoff, L., Bischl, B., 2019. mlr3: A modern object-oriented machine learning framework in R. Journal of Open Source Software 4, 1903. doi:10.21105/joss.01903.

Maudsley, A.A., Domenig, C., Govind, V., Darkazanli, A., Studholme, C., Arheart, K., Bloomer, C., 2009. Mapping of Brain Metabolite Distributions by Volumetric Proton MR Spectroscopic Imaging (MRSI). Magn. Reson. Med. 61, 548–559. doi:10.1002/mrm.21875.

McLaurin, J., Kierstead, M.E., Brown, M.E., Hawkes, C.A., Lambermon, M.H.L., Phinney, A.L., Darabie, A.A., Cousins, J.E., French, J.E., Lan, M.F., Chen, F., Wong, S.S.N., Mount, H.T.J., Fraser, P.E., Westaway, D., St George-Hyslop, P., 2006. Cyclohexanehexol inhibitors of Abeta aggregation prevent and reverse Alzheimer phenotype in a mouse model. Nat. Med. 12, 801–808. doi:10.1038/nm1423.

Mescher, M., Merkle, H., Kirsch, J., Garwood, M., Gruetter, R., 1998. Simultaneous in vivo spectral editing and water suppression. NMR Biomed. 11, 266–272. doi:10.1002/(sici)1099-1492(199810)11:6<266::aid-nbm530>3.0.co;2-j.

Near, J., Harris, A.D., Juchem, C., Kreis, R., Marjańska, M., Öz, G., Slotboom, J., Wilson, M., Gasparovic, C., 2021. Preprocessing, analysis and quantification in single-voxel magnetic resonance spectroscopy: experts' consensus recommendations. NMR Biomed. 34, e4257. doi:10.1002/nbm.4257.

Nikolaidis, A., Baniqued, P.L., Kranz, M.B., Scavuzzo, C.J., Barbey, A.K., Kramer, A.F., Larsen, R.J., 2017. Multivariate Associations of Fluid Intelligence and NAA. Cereb. Cortex 27, 2607–2616. doi:10.1093/cercor/bhw070.

Oz, G., Alger, J.R., Barker, P.B., Bartha, R., Bizzi, A., Boesch, C., Bolan, P.J., Brindle, K.M., Cudalbu, C., Dinçer, A., Dydak, U., Emir, U.E., Frahm, J., González, R.G., Gruber, S., Gruetter, R., Gupta, R.K., Heerschap, A., Henning, A., Hetherington, H.P., Howe, F.A., Hüppi, P.S., Hurd, R.E., Kantarci, K., Klomp, D.W.J., Kreis, R., Kruiskamp, M.J., Leach, M.O., Lin, A.P., Luijten, P.R., Marjańska, M., Maudsley, A.A., Meyerhoff, D.J., Mountford, C.E., Nelson, S.J., Pamir, M.N., Pan, J.W., Peet, A.C., Poptani, H., Posse, S., Pouwels, P.J.W., Ratai, E.-M., Ross, B.D., Scheenen, T.W., Schuster, C., Smith, I.C.P., Soher, B.J., Tkáč, I., Vigneron, D.B., Kauppinen, R.A.MRS Consensus Group, 2014. Clinical proton MR spectroscopy in central nervous system disorders. Radiology 270, 658–679. doi:10.1148/radiol.13130531.

Öz, G., Deelchand, D.K., Wijnen, J.P., Mlynárik, V., Xin, L., Mekle, R., Noeske, R., Scheenen, T.W.J., Tkáč, I., 2021. Advanced single voxel 1H magnetic resonance spectroscopy techniques in humans: Experts' consensus recommendations. NMR in Biomedicine 34, e4236. doi:10.1002/nbm.4236.

Patrick, C.J., Curtin, J.J., Tellegen, A., 2002. Development and validation of a brief form of the Multidimensional Personality Questionnaire. Psychol. Assess. 14, 150–163. doi:10.1037//1040-3590.14.2.150.

Puts, N.A.J., Edden, R.A.E., Evans, C.J., McGlone, F., McGonigle, D.J., 2011. Regionally specific human GABA concentration correlates with tactile discrimination thresholds. J. Neurosci. 31, 16556–16560. doi:10.1523/JNEUROSCI.4489-11.2011.

R Core Team, 2021. R: A Language and Environment for Statistical Computing.

Sanz, M.L., Villamiel, M., Martínez-Castro, I., 2004. Inositols and carbohydrates in different fresh fruit juices. Food Chemistry 87, 325–328. doi:10.1016/j.foodchem.2003.12.001.

Schubert, F., Gallinat, J., Seifert, F., Rinneberg, H., 2004. Glutamate concentrations in human brain using single voxel proton magnetic resonance spectroscopy at 3 Tesla. Neuroimage 21, 1762–1771. doi:10.1016/j.neuroimage.2003.11.014.

Seaquist, E.R., Gruetter, R., 1998. Identification of a high concentration of scyllo-inositol in the brain of a healthy human subject using 1H- and 13C-NMR. Magn. Reson. Med. 39, 313–316. doi:10.1002/mrm.1910390220.

Smith, S.M., Nichols, T.E., Vidaurre, D., Winkler, A.M., Behrens, T.E.J., Glasser, M.F., Ugurbil, K., Barch, D.M., Van Essen, D.C., Miller, K.L., 2015. A positive-negative mode of population covariation links brain connectivity, demographics and behavior. Nature Neuroscience 18, 1565–1567. doi:10.1038/nn.4125.

Stagg, C.J., Bachtiar, V., Johansen-Berg, H., 2011. The role of GABA in human motor learning. Curr. Biol. 21, 480–484. doi:10.1016/j.cub.2011.01.069.

Sumner, P., Edden, R.A.E., Bompas, A., Evans, C.J., Singh, K.D., 2010. More GABA, less distraction: a neurochemical predictor of motor decision speed. Nat. Neurosci. 13, 825–827. doi:10.1038/nn.2559.

Tuch, D.S., Salat, D.H., Wisco, J.J., Zaleta, A.K., Hevelone, N.D., Rosas, H.D., 2005. Choice reaction time performance correlates with diffusion anisotropy in white matter pathways supporting visuospatial attention. Proc. Natl. Acad. Sci. U. S. A. 102, 12212–12217. doi:10.1073/pnas.0407259102.

Urenjak, J., Williams, S.R., Gadian, D.G., Noble, M., 1993. Proton nuclear magnetic resonance spectroscopy unambiguously identifies different neural cell types. J. Neurosci. 13, 981–989.

van Gaal, S., Scholte, H.S., Lamme, V.A.F., Fahrenfort, J.J., Ridderinkhof, K.R., 2011. Pre-SMA graymatter density predicts individual differences in action selection in the face of conscious and unconscious response conflict. J. Cogn. Neurosci. 23, 382–390. doi:10.1162/jocn.2010.21444.

Velazquez, R., Ferreira, E., Knowles, S., Fux, C., Rodin, A., Winslow, W., Oddo, S., 2019. Lifelong choline supplementation ameliorates Alzheimer's disease pathology and associated cognitive deficits by attenuating microglia activation. Aging Cell 18, e13037. doi:10.1111/acel.13037.

Viola, A., Nicoli, F., Denis, B., Confort-Gouny, S., Le Fur, Y., Ranjeva, J.-P., Viout, P., Cozzone, P.J., 2004. High cerebral scyllo-inositol: a new marker of brain metabolism disturbances induced by chronic alcoholism. MAGMA 17, 47–61. doi:10.1007/s10334-004-0044-x.

Wang, Y., Li, S.-J., 1998. Differentiation of metabolic concentrations between gray matter and white matter of human brain by in vivo 1H magnetic resonance spectroscopy. Magnetic Resonance in Medicine 39, 28–33. doi:10.1002/mrm.1910390107.

White, T.L., Gonsalves, M.A., Cohen, R.A., Harris, A.D., Monnig, M.A., Walsh, E.G., Nitenson, A.Z., Porges, E.C., Lamb, D.G., Woods, A.J., Borja, C.B., 2021. The neurobiology of wellness: 1H-MRS correlates of agency, flexibility and neuroaffective reserves in healthy young adults. Neuroimage 225, 117509. doi:10.1016/j.neuroimage.2020.117509.

Wilson, M., 2021a. spant: An R package for magnetic resonance spectroscopy analysis. JOSS 6, 3646. doi:10.21105/joss.03646.

Wilson, M., 2021b. Adaptive baseline fitting for 1H MR spectroscopy analysis. Magn. Reson. Med. 85, 13–29. doi:10.1002/mrm.28385.

Wilson, M., 2019. Robust retrospective frequency and phase correction for single-voxel MR spectroscopy. Magn. Reson. Med. 81, 2878–2886. doi:10.1002/mrm.27605.

Wilson, M., Andronesi, O., Barker, P.B., Bartha, R., Bizzi, A., Bolan, P.J., Brindle, K.M., Choi, I.-Y., Cudalbu, C., Dydak, U., Emir, U.E., Gonzalez, R.G., Gruber, S., Gruetter, R., Gupta, R.K., Heerschap, A., Henning, A., Hetherington, H.P., Huppi, P.S., Hurd, R.E., Kantarci, K., Kauppinen, R.A., Klomp, D.W.J., Kreis, R., Kruiskamp, M.J., Leach, M.O., Lin, A.P., Luijten, P.R., Marjańska, M., Maudsley, A.A., Meyerhoff, D.J., Mountford, C.E., Mullins, P.G., Murdoch, J.B., Nelson, S.J., Noeske, R., Öz, G., Pan, J.W., Peet, A.C., Poptani, H., Posse, S., Ratai, E.-M., Salibi, N., Scheenen, T.W.J., Smith, I.C.P., Soher, B.J., Tkáč, I., Vigneron, D.B., Howe, F.A., 2019. Methodological consensus on clinical proton MRS of the brain: Review and recommendations. Magn. Reson. Med. 82, 527–550. doi:10.1002/mrm.27742.

Wilson, M., Reynolds, G., Kauppinen, R.A., Arvanitis, T.N., Peet, A.C., 2011. A constrained least-squares approach to the automated quantitation of in vivo ^{1}H magnetic resonance spectroscopy data. Magn. Reson. Med. 65, 1–12. doi:10.1002/mrm.22579.

Woolrich, M.W., Jbabdi, S., Patenaude, B., Chappell, M., Makni, S., Behrens, T., Beckmann, C., Jenkinson, M., Smith, S.M., 2009. Bayesian analysis of neuroimaging data in FSL. Neuroimage 45, S173–S186. doi:10.1016/j.neuroimage.2008.10.055.

Ylilauri, M.P.T., Voutilainen, S., Lönnroos, E., Virtanen, H.E.K., Tuomainen, T.-P., Salonen, J.T., Virtanen, J.K., 2019. Associations of dietary choline intake with risk of incident dementia and with cognitive performance: the Kuopio Ischaemic Heart Disease Risk Factor Study. Am. J. Clin. Nutr. 110, 1416–1423. doi:10.1093/ajcn/nqz148.

Zhang, Y., Brady, M., Smith, S., 2001. Segmentation of brain MR images through a hidden Markov random field model and the expectation-maximization algorithm. IEEE Trans. Med. Imaging 20, 45–57. doi:10.1109/42.906424.